Numerical simulations of the pulsating flow of cerebrospinal fluid flow in the cervical spinal canal of a Chiari patient

Anders Helgeland^a, Kent-Andre Mardal^b, Victor Haughton^{b,c}, Bjørn Anders Pettersson Reif^{a,d,e}

^aNorwegian Defence Research Establishment (FFI), Kjeller, NORWAY
 ^bCenter for Biomedical Computing, Simula Research Laboratory, Fornebu, NORWAY
 ^cDepartment of Radiology, School of Medicine and Public Health, University of Wisconsin, USA
 ^dDepartment of Mathematics, University of Oslo, Oslo, NORWAY
 ^eUniversity Graduate Center (UniK), Kjeller, NORWAY

Abstract

The flow dynamics of the cerebrospinal fluid (CSF) in a patient-specific model of the subarachniod space in a Chiari I patient were investigated using numerical simulations. The pulsating CSF flow was modeled using a time-varying velocity pulse based on peak velocity measurements (diastole and systole) derived from a selection of patients with Chiari I malformation. The present study used the general definition of the Reynolds number to provide a measure of CSF flow instability to give an estimate of the possibility of turbulence occurring in CSF flow. This was motivated by the fact that the combination of pulsuating flow and the geometric complexity of the spinal canal may result in *local* Reynolds numbers that are significantly higher than the commonly used global measure such that flow instabilities may develop into turbulent flow in these regions. The general or local Reynolds number was used in combination with derived statistics to characterize the flow. The results revealed both local unstable regions and local regions with velocity fluctuations similar in magnitude to what is observed in fully turbulent flows. The results also indicated that the fluctuations were not self-sustained turbulence, but rather flow instabilities that may develop into turbulence. The case considered was believed to represent a CSF flow close to transition.

Keywords: CSF flow, Chiari I, simulations, turbulence, flow instability, local Reynolds number

1. Introduction

10

11

12

14

The Chiari I malformation is a condition characterized by tonsilar herniation through the forman magnum. The herniation obstructs the pulsating flow of cerebrospinal fluid (CSF) through the foramen magnum and is believed to play a key role in the development of syringomyelia that commonly occurs in Chiari I patients. Computational fluid dynamics (CFD) has during the last decade proven itself as a reliable approach to predict complex fluid flow phenomena, and it has therefore become a tool for investigating complex biomedical flows.

The occurrence of complex flow phenomena, including bidirectional flow patterns, in the cervical canal has previously been demonstrated using PC-MR for Chiari I patients [1]. Despite the complexity of the flow, most CSF flow studies rest on the assumption that the flow remains laminar. This is based on a priori estimate of the Reynolds number, based on peak systole velocity and the hydraulic diameter along the spinal canal, which usually lies in the range 150-570. Such a range is considered to be too low for turbulence to occur, c.f. e.g. [2, 3, 4]. Recent 4D PC MR studies [5] however, in which velocities as high as 20 cm/s were reported, have demonstrated that even higher Reynolds numbers can occur.

Previous estimates of the Reynolds-number, and thus also on the *a priori* assumption of laminar flow, are based on a global measure that does not provide information about local variations of the Reynolds-number within the spinal canal. The motivation for this study is that the combination of pulsating flow and the geometric complexity of the canal may result in *local* Reynolds-numbers that are significantly higher than the commonly used global measure such that flow instabilities may develop into chaotic turbulent flow in these regions. The objective of the present study is to use a state-of-the-art CFD methodology to investigate pulsating CSF flow in Chiari I patients in order to provide better understanding of the complexity of flow field, and to provide a measure of CSF flow stability that

estimated the possibility of turbulence in CSF flow. The possibility of turbulent flow in the CSF has not to our knowledge been studied systematically. For this study, we created a 3D model of the spinal subarachnoid space in a Chiari I patient and we assumed CSF flow volumes in the upper range of normal.

2. Mathematical and computational modeling

The present study employs a method that is similar to what is known as direct numerical simulations (DNS) which is a branch of traditional Computational Fluid Dynamics (CFD) devoted to high-fidelity solution of transitional and turbulent flows [6]. This approach differs from conventional CFD in that the turbulence is explicitly resolved rather than being represented by a statistical model. In essence, DNS can be viewed as a numerical experiment that from first principles produces a series of non-empirical solutions representing a virtual three-dimensional and time dependent turbulent or transitional fluid flow. The approach is therefore ideal for addressing basic research questions regarding turbulence physics, but due to the high computational demand and its inherent characteristics DNS has not become a general purpose research tool.

The explicit requirement of a DNS is that all temporal and spatial scales of the flow field are computationally resolved. Turbulence is inherently a multi-scale fluid flow phenomena and it can be shown that the number of degrees-of-freedom of a turbulent flow scales as $N \sim Re^{9/4}$ [7] where Re is the Reynolds-number which typically exceeds $O(10^3)$ in turbulent flows¹. Due to the extreme computational costs, the applicability of DNS is limited to low Reynolds-number flows only which makes it a potentially viable approach in biomedical applications. A still unresolved issue, however, is that all inflow/outflow boundary conditions must be properly prescribed (in time and three-dimensional space). Lacking this information makes the application of DNS in biomedical flows challenging, and special attention has to be taken to ensure minimum influence of this error. Since the CSF flow considered in this study is subjected to an oscillatory motion, this issue were handled by defining the size of the computational domain such that the inflow/outflow boundaries had very small influence on the results in the area of interest.

2.1. Governing equations

24

25

27

28

30

31

32

35

37

39

40

41

43

49

51

52

53

54

56

57

61

The equations governing the flow of an incompressible Newtonian fluid, such as CSF flow, are based on the fundamental principles of conservation of mass and momentum which can be written as

$$\frac{\partial \tilde{u}_i(\mathbf{x},t)}{\partial t} + \tilde{u}_k(\mathbf{x},t) \frac{\partial \tilde{u}_i(\mathbf{x},t)}{\partial x_k} = \nu \frac{\partial^2 \tilde{u}_i(\mathbf{x},t)}{\partial x_k \partial x_k} - \frac{1}{\rho} \frac{\tilde{p}(\mathbf{x},t)}{\partial x_i}, \qquad (1)$$

$$\frac{\partial \tilde{u}_i(\mathbf{x},t)}{\partial x_i} = 0.$$

$$\frac{\partial \tilde{u}_i(\mathbf{x},t)}{\partial r_i} = 0. \tag{2}$$

These are commonly referred to as the Navier-Stokes equations. Here $\tilde{u}_i(\mathbf{x},t)$ denotes the instantaneous velocity component in the x_i direction, $\tilde{p}(\mathbf{x},t)$ is the instantaneous pressure, and ρ is the fluid density whereas $\nu = \mu/\rho$ denotes the kinematic viscosity and μ is the molecular viscosity. We apply the notation $[x_1, x_2, x_3] = [x, y, z]$, cf. figure 1, and $[\tilde{u}_x, \tilde{u}_y, \tilde{u}_z] = [\tilde{u}, \tilde{v}, \tilde{w}]$. Einsteins summation convention also applies, i.e. summation over repeated indices, e.g. $\partial \tilde{u}_i/\partial x_i = \partial \tilde{u}_1/\partial x_1 + \partial \tilde{u}_2/\partial x_2 + \partial \tilde{u}_3/\partial x_3$.

The CSF fluid is assumed to have the physical properties as water at 37 degrees C, i.e. ρ = $1000 \ [kg/m^3]$ and $\nu = 0.7 * 10^{-6} \ [m^2/s]$. Gravity is neglected from equation 1 since its effect is implicitly contained in the inlet velocity boundary conditions which is obtained indirectly from measured

2.2. Numerical simulations

From the registry of Chiari patients at the University of Wisconsin, with approval of the local Institational Review Board, a patient with Chiari I and with evidence of elevated CSF velocities was chosen for the patient-specific modeling. A 3D high-resolution volume MR sequence of the cervical spine and lower posterior fossa showing the subarachnoid space with high contrast resolution was used to create a patient-specific surface model of the spinal canal. The surface model was created using the Vascular

¹In most applications $Re \sim O(10^3) - O(10^9)$

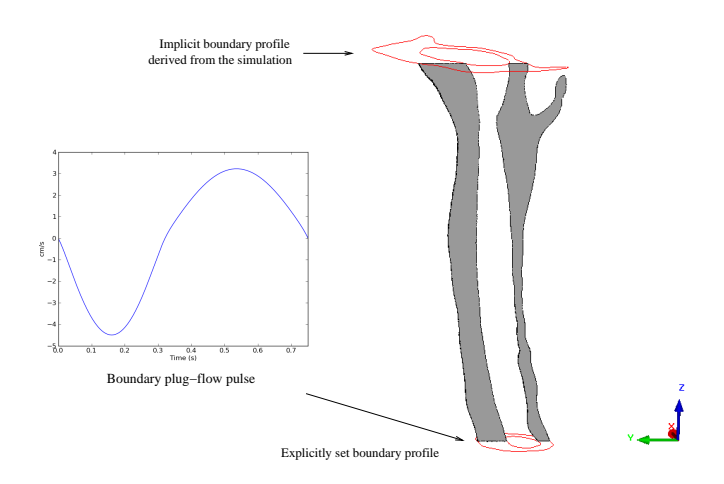


Figure 1: The computational domain $[0.0916 \le x \le 0.129, 0.0769 \le y \le 0.1129, 0.03175 \le z \le 0.106]$ and the velocity CSF boundary pulse.

Modeling Toolkit [8]. Figures 1 and 2 show the three-dimensional geometry of the spinal canal used in the present study. The three-dimensional and time dependent Navier-Stokes equations (1) - (2) were solved using an unstructured finite volume code based on second-order accurate discretization in time and space, cf. [9].

2.2.1. Boundary conditions

The pulsating CSF flow in the subarachnoid space was simulated using a time varying velocity pulse defined at the lower boundary of the computational domain (see fig 1). The form of the pulse varies from case to case, but in general the systolic phase of the flow (downward fluid movement) has a greater amplitude and a shorter period compared to the diastolic phase (upward fluid movement). The CSF flow pulse used in this study was generated to agree with the peak velocity amplitudes derived from a selection of patients with Chiari I malformation measured by Shah et. al. [10], cf. figure 1. The pulse was generated to produce maximum systolic and diastolic velocities around 10 cm/s and 7.5 cm/s, respectively, with a cycle of = 0.75 seconds. This corresponds to a heart rate of 80 beats per minute. Figure 2 shows the modeled spinal channel. The outer (and inner) boundaries of the spinal canal were assumed to be rigid and therefore modeled using no-slip boundary conditions, i.e. $\tilde{u}_i = 0$, for all i.

Since the flow direction reverses during each cycle, special care has to be taken to minimize any influence of the inflow/outflow boundaries on the flow field within the region of interest. The computational model was therefore geometrically extended from the upper and lower boundary surfaces. The extension was designed to prevent flow structures created within the spinal channel to be affected by the computational boundaries. The reason that this could happen is that the imposed velocity field at the boundaries is assumed to be one-componential and unidirectional (i.e. the only non-zero velocity component being that perpendicular to the inflow plane), whereas flow structures in general are three-dimensional and three-componential ($\tilde{u}_i(x,y,z,t) \neq 0$). A three-dimensional flow structure that is advected through the boundary would no longer be present when the flow reverses. The terminology "one-componential" alludes to a velocity field with only one non-zero component, whereas all three velocity components generally are non-zero in a "three-componential" field.

The length of extension was estimated by considering the length a particle near the original boundary surfaces would travel on average in the oscillating CSF flow during one cycle. Using the boundary plugflow pulse as a mean velocity measure gives us an average traveled distance of approximately 0.9 cm (in both systole and diastole). This distance can be used as an upper limit near the upper boundary wall since the upper surface has a greater area and therefore lower velocities on average. Based on this estimate, we extended the upper surface by 1 cm and the lower by 3 cm. It should be noted that the cross-sectional area is smaller in the lower part of the geometry which implies higher velocities. The geometrical extensions were thus added to the model to minimize the influence of the explicit boundary condition on the flow field within the originally segmented geometry. The analysis presented here are based only on the computed flow field within the originally segmented spinal channel. The complete

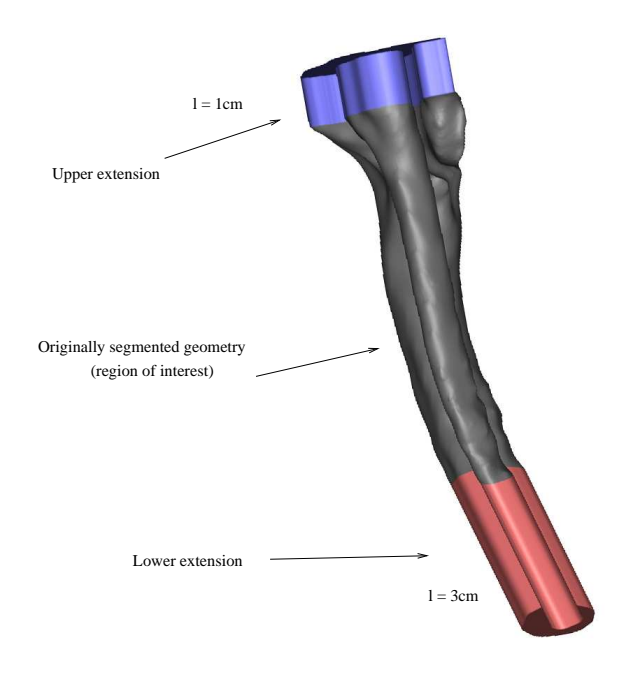


Figure 2: Expansion of the originally segmented model of the spinal canal.

computational model, including the region of interest, is shown in figure 2.

2.2.2. Computational mesh

The simulations were run using a computational mesh consisting of approximately 46.5 million volume cells. Special care was taken to ensure that the grid density was fine enough to resolve spatial flow structures that may appear. The most common estimate of the smallest flow scales is based on the Kolmogorov scale estimates [11]. According to Kolmogorov, the smallest scales that can persist in a time-dependent flow has a length $\eta \sim \nu/u_*$ where u_* is the local frictional velocity and ν is the kinematic viscosity of the fluid. The local friction velocity is defined as $u_* = \sqrt{2\nu|S_{ij}S_{ij}|^{1/2}}$ where $S_{ij} = 1/2 (\partial \tilde{u}_i/\partial x_j + \partial \tilde{u}_j/\partial x_i)$ is the symmetric part of the velocity gradient tensor.

The quality of the grid resolution was then estimated by considering the ratio between the averaged grid size, $\Delta l = \Delta_{vol}^{1/3}$ where Δ_{vol} is the volume of the computational cell, and the Kolmogorov scale, i.e.

$$l^{+} = \frac{u_* \Delta l}{\nu}.\tag{3}$$

Ideally, this ratio should be less than unity but in practice $l^+ \sim \mathcal{O}(10)$ usually suffices, cf. [6].

Similarly, the computational time step, Δt , required to resolve the most rapidly varying structures can be estimated by considering the ratio between the time step (Δt) and corresponding Kolmogorov time scale $\tau = \nu/u_*^2$, i.e.

$$t^{+} = \frac{\Delta t u_*^2}{\nu}.\tag{4}$$

In this study we have used $\Delta t = 0.00075$ s.

It should be noted that l^+ and t^+ are both a priori unknown since the friction velocity depends on the solution. These checks can therefore only be performed after the simulation is completed. It is however important to also notice that since these measures depends on the size of the computational grid, and the selected time step, the computed values of l^+ and t^+ only serve as an indirect measure of the quality of the computation. This procedure is nevertheless very valuable assessing the quality of the simulation setup. The results presented here produce $l^+ \leq 2.4$ and $t^+ \leq 0.66$ within the spinal channel. This confirms that the current simulations were conducted using sufficient spatial and temporal resolution in order to properly resolve the smallest expected structures of the flow field.

2.3. Flow instabilities

118

119

120

121

122

123

125

130

The flow inside the spinal canal develops into a complex fully three-dimensional field. The nonlinearity of the Navier-Stokes equations, represented by the advection term in equation 1, tends to trigger instabilities that eventually may develop into a fully turbulent state. A frequently used approach to make an a priori assessment if the flow is turbulent or not, is to consider the so-called Reynolds number (Re); if the Reynolds number exceeds a certain critical value, $Re > Re_{critical}$, turbulent flow is likely to occur. There exists however no generally applicable number $Re_{critical}$ since the exact value varies from case to case. This means that in order to identify possible regions were flow instabilities may occur, a different method is needed.

Let us consider the Reynolds number based on its most general definition, i.e. as the ratio between the inertia and viscous forces. For the flow in the x_i -direction this ratio is given by

$$Re_{i} = \frac{\rho(\partial \tilde{u}_{i}/\partial t + \tilde{u}_{m}\partial \tilde{u}_{i}/\partial x_{m})}{\mu(\partial^{2}\tilde{u}_{i}/(\partial x_{k}\partial x_{k}))}$$

$$(5)$$

with no summation over the repeated index i, cf. also (1). Considering a three-dimensional flow, the magnitude of this ratio defines the general or local Reynolds-number Re_g , i.e. $Re_g(\mathbf{x},t) = (Re_1^2 + Re_2^2 + Re_3^2)^{1/2}$ which varies locally in the flow². The notion of a critical Reynolds number comes from the fact that if the (destabilizing) inertia forces are large enough compared to the (stabilizing) viscous forces, instabilities are able to grow in time without being damped by viscous effects.

2.4. Statistical description

The flow field was simulated during 29 heartbeats, corresponding to 29 cycles of CSF flow. For each time step during each cycle the numerical solution of equations (1) and (2) with the given boundary conditions provide the instantaneous three-dimensional velocity and pressure fields inside the spinal canal. In order to facilitate a meaningful flow field analysis, the instantaneous velocity field is decomposed into a mean and a fluctuating part, i.e. $\tilde{u}_i(\mathbf{x},t) = U_i(\mathbf{x},t) + u_i(\mathbf{x},t)$ which are obtained as

$$U_i(\mathbf{x},t) = \langle \tilde{u}_i(\mathbf{x},t) \rangle_{N_1} \tag{6}$$

and

133

134

135

139

$$u_i(\mathbf{x},t) = \tilde{u}_i(\mathbf{x},t) - \langle \tilde{u}_i(\mathbf{x},t) \rangle_{N_1}, \tag{7}$$

respectively, where $\langle ... \rangle_N$ represents the point-wise phase averaged correlation using N cycles. The simulation was first run for 10 cycles in order to establish a fully developed flow field before the averaging procedure commenced. In order to obtain a statistically converged mean flow field $N_1 = 10$ was used.

The fluctuating velocity field is analyzed using the single-point second-order moment:

$$R_{ij}(\mathbf{x},t) = \langle u_i(\mathbf{x},t)u_j(\mathbf{x},t)\rangle_{N_2}.$$
 (8)

This correlation is commonly referred to as the components of the Reynolds stress (R_{ij}) tensor. $R_{ij}(\mathbf{x},t)$ physically represents the effect of the phase averaged fluctuating velocity components on the mean flow field. Here, $N_2 = 9$ was judged to constitute a sufficient number of cycles in order to obtain converged statistics in the present case. Statistics were sampled at 6 discrete time points during the heart-beat cycle, cf. figure 3.

The physical characterization of the Reynolds-stress tensor has been carried out using:

$$\Lambda(\mathbf{x},t) = \frac{R_{ii}}{R_{kk} + U_j U_j} \tag{9}$$

and

$$II_a(\mathbf{x},t) = -\frac{1}{2}b_{ij}b_{ji},\tag{10}$$

²It should be noted that the local Reynolds number as defined in (5) can become pointwise singular within the computational domain, thus displaying very large local values. The pointwise extremes are however not associated with *regions* at which local instabilities can occur.

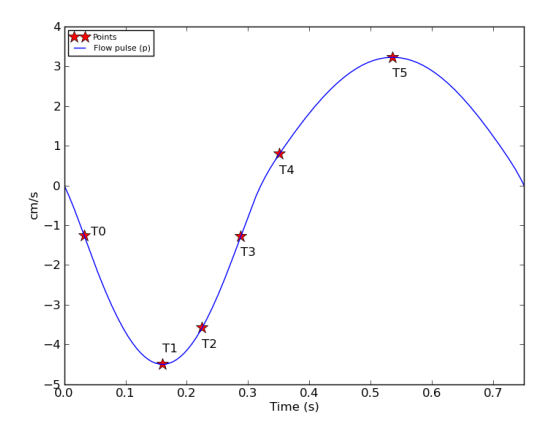


Figure 3: The boundary plug-flow pulse together with six discrete sample points during the heart-beat cycle in which statistics were sampled.

where $\Lambda(\mathbf{x},t)$ is a measure of the ratio between the fluctuating and the total kinetic energy. Here R_{ii} and U_jU_j denote (twice) the kinetic energy (per unit mass) of the fluctuating and mean flow field, respectively. $II_a(\mathbf{x},t)$ is the second invariant of the Reynolds-stress anisotropy tensor ($b_{ij}=2R_{ij}/R_{kk}-2\delta_{ij}/3$) and it is used to characterize the kinematical structure of the fluctuating flow field. Mathematically, II_a is a measure of the departure from isotropic fluctuations, i.e. fluctuations that are statistically the same in all directions ($R_{11}^{1/2}=R_{22}^{1/2}=R_{33}^{1/2}$). From its definition (10), the following limits can be analytically deduced: $II_a=0$ represents isotropic fluctuations; $II_a=-2/3$ indicates that no fluctuations are present, and $II_a=-4/3$ represents so-called 'one-componential' (1-C) fluctuations, i.e. that the fluctuations only occur in one directions, e.g. $R_{11}^{1/2}=R_{22}^{1/2}=0$ and $R_{33}^{1/2}\neq0$. The 1-C case represents a physical state where fluctuations occur but the flow has not yet been developed into full turbulence (which must have fluctuations in all directions in order to remain self-sustained).

3. Results

Phase averaged statistics were computed at six discrete times $(T_0 - T_5)$ during each cycle, cf. figure 3. Figure 4 displays contours of the vertical (z) component of the mean velocity in a vertical plane cutting across the spinal channel at different (time) points during the cycle. Figure 5 shows the corresponding mean velocity (U_z) contours in a horizontal plane near the Chiari I malformation. The results demonstrate the complexity of the CSF flow field. Flow along the spinal axis occurs synchronously in positive and negative vertical direction at several instances throughout the CSF cycle $(t = T_0, t = T_3, \text{ and } t = t_4)$ as can be seen from figure 5. There is also a time lag between the directional changes of the inflow velocity profile at the lower boundary and the changes of the flow field within the spinal channel. This can for instance be observed by investigating figure 4, at $t = T_4$, which clearly reveals local regions with opposite velocity direction (compared to the inflow pulse) that prevails for a periode of time after the inflow velocity pulse changes direction.

In order to identify regions of the CSF flow that may develop instabilities, the general or local Reynolds-number $(Re_g(\mathbf{x},t))$ has been computed. The result indicates that the most unstable region of the flow is located in the vicinity of the Chiari I malformation. This is exemplified in figures 6(a) and 6(b) where contours of $Re_g(\mathbf{x},t)$ at $t=T_0$ are shown on a vertical and a horizontal plane, respectively. Large values (> 2000) can be observed in the vicinity of the malformation which means that the (destabilizing) inertia forces acting on the fluid in this particular region are much larger than the corresponding (stabilizing) viscous forces; instabilities are therefore likely to develop in this particular region that may trigger velocity fluctuations. Similar results are also found at $t=T_3$ in regions nearby the malformation. Somewhat similar but not as pronounced results also occurred for the other sampled time instances.

Figure 7 displays contours of the fluctuating and mean kinetic energy ratio parameter $\Lambda(\mathbf{x}, t)$, cf. (9), at $t = T_0$, $t = T_3$, and $t = T_4$ in a horizontal plane close to the malformation. The results indicate that strong velocity fluctuations, relative to the local mean velocity magnitude, occur in the spinal channel

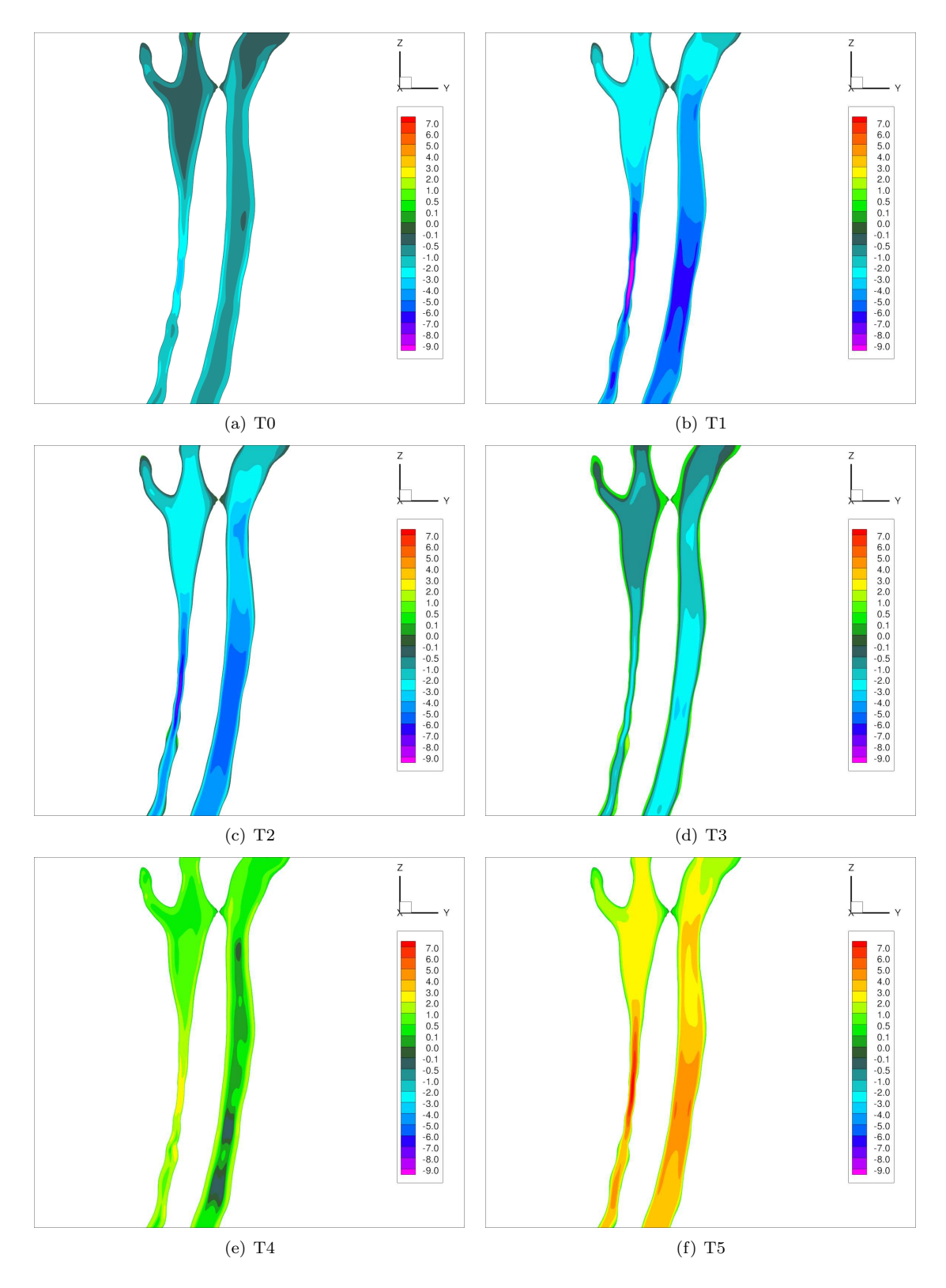


Figure 4: Contours of the vertical (z) component of the mean velocity (cm/s) for six time samples in a vertical (y,z) plane at x = 0.101. The color tables are fixed for all images with green, yellow and red colors representing positive values and with grey, dark blue, cyan, blue and magenta colors representing negative values.

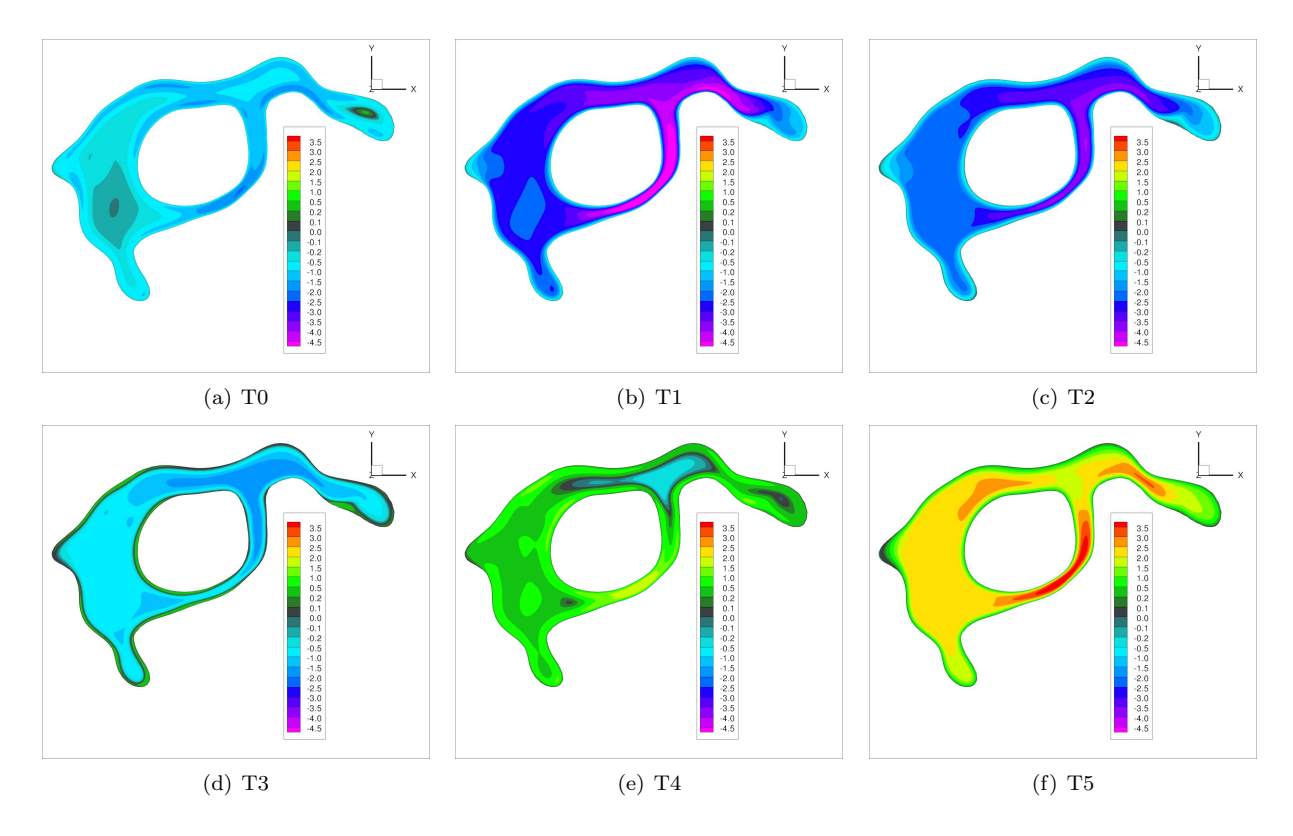


Figure 5: Contours of the vertical (z) component of the mean velocity for six time samples in a horizontal (x,y) plane at z = 0.097. The color tables are fixed for all images with green, yellow and red colors representing positive values and with cyan, blue and magenta colors representing negative values.

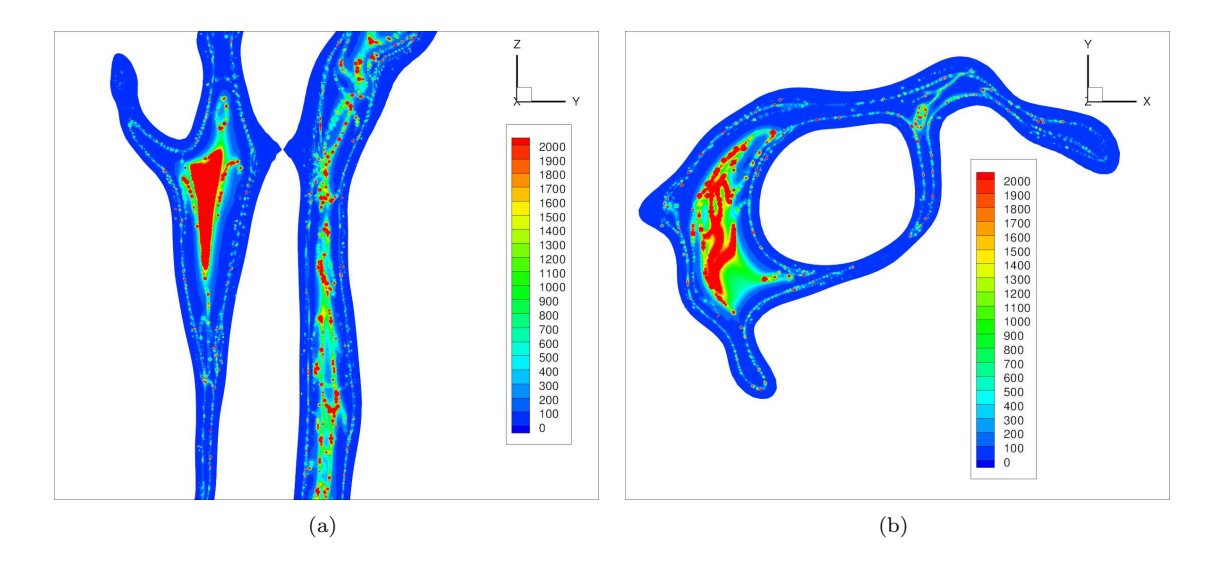


Figure 6: Contours of the General Reynolds number for a vertical plane (a), at x = 0.101, and a horizontal plane (b), at z = 0.097, both at $t = T_0$.

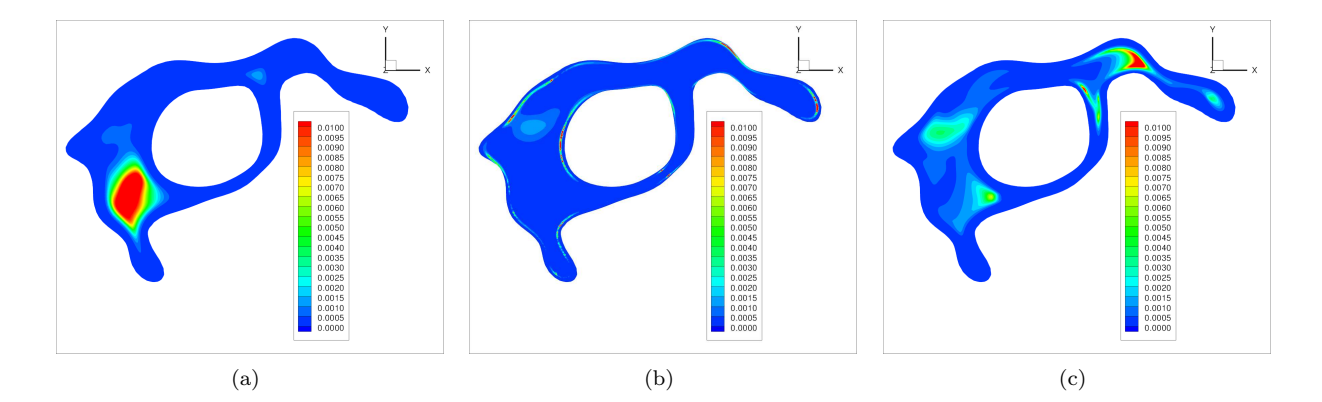


Figure 7: Contours of the ratio $\Lambda = R_{ii}/(R_{kk} + U_j U_j)$ for $t = T_0$ (a), $t = T_3$ (b) and $t = T_4$ (c) in a horizontal (y,z) plane, at z = 0.097, in vicinity of the Chiari I malformation. In red areas, the velocity fluctuations are 10% (or higher) relative to the local mean velocity magnitude. Note that the plotted values of Λ are squared values, meaning that values close to 0.01 corresponds to fluctuations around 10% of the mean velocity.

close to the malformation; 10 - 20 % of U_z . This is not so evident for the other time instances considered here. In other regions of the spinal channel the fluctuations are in general very small (but finite), with the exception of a few small areas with relatively high levels of fluctuations.

The simulation results also indicate that the second invariant $II_a \approx -4/3$ across most of the spinal channel, also in the vicinity of the malformation where the strongest fluctuations occur. This implies that the *fluctuating* velocity field is nearly one-componential and thus is not fully turbulent. Despite its one-componential nature, a non-zero correlation between the vertical fluctuation and the fluctuation in the horizontal plane could be observed. This is an indication that the flow field is close to transition.

4. Conclusions

The numerical simulation presented in this study has revealed that the oscillating CSF flow in the spinal channel is very complex. The flow field is fully three-dimensional and exhibits regions with opposing flow directions during a significant portion of the CSF cycle. These opposing flow structures contribute significantly to the dynamics of the CSF flow, including the observed time lag between the inflow time variation and the local temporal response of the mean flow in the spinal channel.

The present study has utilized the fundamental definition of the Reynolds-number to reveal the most unstable regions of the flow. To the knowledge of the authors this is the first time this definition is used in the literature for the purpose of analyzing local Reynolds-numbers. It was demonstrated that the most significant region of unstable flow in the spinal channel is located in the immediate vicinity of the malformation. In this region, one-componential velocity fluctuations developed with magnitude 10-20% of the local mean flow magnitude which is similar to what can be observed in fully turbulent flows. The results also indicate that the fluctuations are not self-sustained turbulence, but rather flow instabilities that eventually may develop into a turbulence.

The case considered in this study is believed to represent a CSF flow that is very close to turbulence transition. Firstly, a modest increase of inflow velocity magnitude and/or frequency may be enough to initially trigger turbulence in the immediate vicinity of the malformation, and then also across the entire spinal channel. Secondly, the "nerve roots" that stretches across the spinal channel have been neglected in the present study; these inherently introduce flow disturbances that may influence the dynamics of the CSF flow and cause turbulence transition to occur.

5. Conflict of interest statement

There is no conflict of interest for all authors

206 6. Acknowledgments

This work was supported in part by Column of Hope.

08 References

- [1] M. F. Quigley, B. J. Iskandar, M. A. Quigley, M. N. Nicosia, V. Haughton, Cerebrospinal fluid flow in foramen magnum: Temporal and spatial patterns at MR imaging in volunteers and in patients with Chiari I malformation, Radiology 232 (2004) 229–236.
- [2] F. Loth, M. A. Yardimci, N. Alperin, Hydrodynamic modeling of cerebrospinal fluid motion within the spinal cavity, J. Biomech. Eng. 123 (2001) 71–79.
- 214 [3] S. Linge, V. Haughton, A. E. Løvgren, K.-A. Mardal, H. P. Langtangen, CSF flow dynamics at the craniovertebral junction studied with an idealized model of the subarachnoid space and computational flow analysis, American Journal of Neuroradiology 31 (1) (2010) 185–192.

 URL http://dx.doi.org/10.3174/ajnr.A1766
- ²¹⁸ [4] S. Linge, V. Haughton, A. E. Løvgren, K.-A. Mardal, A. Helgeland, H. P. Langtangen, Effect of tonsillar herniation on cyclic csf flow studied with computational flow analysis, American Journal of Neuroradiology 32 (8) (2011) 1474–1481.
- [5] A. C. Bunck, J. R. Kroeger, A. Juettner, A. Brentrup, B. Fiedler, G. R. Crelier, B. A. Martin,
 W. Heindel, D. Maintz, W. Schwindt, T. Niederstadt, Magnetic resonance 4d flow analysis of cere brospinal fluid dynamics in chiari i malformation with and without syringomyelia, European Radiology 22 (9) (2012) 1860–1870.
- ²²⁵ [6] P. Moin, K. Mahesh, Direct numerical simulation: A tool in turbulence research, Annu. Rev. Fluid Mech. 30 (1) (1998) 539–578.
- 227 [7] N. D. Sandham, Closure strategies for turbulent and transitional flows, Cambridge University Press, 2002, Ch. Introduction to direct numerical simulations.
- 229 [8] Vascular Modeling Toolkit, http://www.vmtk.org.
- [9] CDP, http://www.stanford.edu/group/cits/research/combustor/cdp.html.
- [10] S. Shah, V. Haughton, A. del Ro, CSF flow through the upper cervical spinal canal in chiari i malformation., AJNR Am J Neuroradiol 32 (6) (2011) 1149–53.
- ²³³ [11] P. Durbin, B. A. P. Reif, Statistical Theory and Modeling for Turbulent Flows, John Wiley and Sons, 2010.